ELSEVIER

Mechanisms of Development 119S (2002) S161–S166

www.elsevier.com/locate/modo

Isolation and expression of two zebrafish homologues of *parvalbumin* genes related to chicken *CPV3* and mammalian *oncomodulin*

Chung-Der Hsiao, Wei-Yuan Tsai, Huai-Jen Tsai*

Institute of Fisheries Science, National Taiwan University, Section 4,1 Roosevelt Road, Taipei 106, Taiwan, ROC

Received 16 July 2002; received in revised form 23 August 2002; accepted 27 August 2002

Abstract

Full-length cDNA clones coded for two β-type homologues of *parvalbumin* genes, *pvalb3a* and *pvalb3b*, were isolated from zebrafish. The homology and phylogenetic analyses, based on the deduced amino acid sequences, revealed that PVALB3A and PVALB3B are co-orthologues to chicken CPV3 and mammalian oncomodulin (OCM) but are divergent from α-type PVALB of tetrapods and muscle-type PVALB of bony fish. Whole-mount in situ hybridization revealed that the spatio-temporal expression of *pvalb3a* and *pvalb3b* were distinct and highly development-regulated during early embryogenesis. Unlike their counterparts of *CPV3* in chicken and *OCM* in mammals, zebrafish *pvalb3a* transcripts were widely expressed in mucous cells, the olfactory epithelium, anterior pituitary, pharyngeal teeth germ, macrophages, inner ear and lateral line neuromasts, whereas, *pvalb3b* transcripts were more restrictedly expressed in the yolk syncytial layer, inner ear and pronephric ducts.

Keywords: Ca^{2+} binding proteins; Parvalbumin; Zebrafish; Embryogenesis

1. Results and discussion

The parvalbumin (PVALB) is a small, vertebrate-specific member of the troponin C superfamily. It contains two functional Ca^{2+} binding sites, commonly referred to as the CD and EF binding sites. Both sites typically belong to the 'high-affinity' or 'Ca^{2+}/Mg^{2+}' category, exhibiting substantial affinity for both Ca^{2+} and Mg^{2+} ions at physiological pH and ionic strength. PVALB is generally viewed as a Ca^{2+} buffer that probably functions as a soluble relaxing factor and cytosolic Ca^{2+} ion reservoir (reviewed by Pauls et al., 1996). Based on amino acid sequences, PVALB is further subdivided into two evolutionary distinct lineages, α- and β-type. In general, the tissue distribution of β-type PVALB is more restricted than that of α-type PVALB in tetrapods. For example, α-type PVALB has been detected in skeletal myofibrils (Gosselin-Rey and Gerday, 1977), endocrine glands (Endo et al., 1985), the brain (de Lecea et al., 1995), bone (Toury et al., 1995) and kidney (Kerschbaum et al., 1994; Loffing et al., 2001). However, in β-lineage, chicken CPV3 is specifically expressed in the thymus (Hapak et al., 1994), and mammalian oncomodulin (OCM) is specifically expressed in the hair cells of the Corti organ (Henzl et al., 1997; Sakaguchi et al., 1998). To substantiate the pivotal role of PVALB in the embryogenesis of lower vertebrates, we cloned two β-type zebrafish homologues of *pvalb3a* and *pvalb3b* related to chicken *CPV3* and mammalian *OCM*.

1.1. Isolation of zebrafish pvalb3a and pvalb3b

Through a BLAST search of the zebrafish expressed sequence tags (EST) database, at least nine distinct and incomplete *pvalb*-like cDNA sequences were identified. Among these nine EST clones, two (accession numbers BE201681 and AW778394) were highly similar to chicken *CPV3*. Full-length cDNAs of these two *CPV3*-like EST clones were obtained through rapid amplification of cDNA ends. Predicted open reading frames of both *CPV3*-like cDNAs consisted of 109 amino acids and pI values of 4.4 and 4.0, respectively. Based on the fact that their pI values were less than 4.5, these two *CPV3*-like *pvalb* belong to β-lineage (Pauls et al., 1996). Homology analysis, based on the deduced amino acid sequences, revealed that both β-type PVALBs shared high identities with chicken CPV3 (60–73%) and mammalian OCM (49–61%) (Fig. 1A). Protein sequence alignment with other β-type PVALBs from bony fish, chicken and mammals revealed that two Ca^{2+}-binding domains characteristic of the EF-hand Ca^{2+} binding protein family and two residues (Arg^{76} and Glu^{82})

* Corresponding author. Tel.: +886-2-2366-1540; fax: +886-2-2363-8483.

E-mail address: hjtsai@ccms.ntu.edu.tw (H.-J. Tsai).

0925-4773/03/$ - see front matter
PII: S0925-4773(03)00110-2

mediating salt-bridge formation were strikingly conserved within all the β-type PVALBs examined (Fig. 1A). Phylogenetic analysis, based on the deduced amino acid sequences, revealed that both β-type zebrafish PVALBs were closely related to chicken CPV3 and mammalian OCM but were divergent from α-type PVALB of tetrapods and muscle-type PVALB of bony fish (Fig. 1B). All this evidence clearly indicated that the two β-type *pvalbs* isolated in this study were indeed orthologues to chicken *CPV3* and mammalian *OCM*. Therefore, we named them zebrafish *pvalb3a* and *pvalb3b* because they are co-orthologues to chicken *CPV3*.

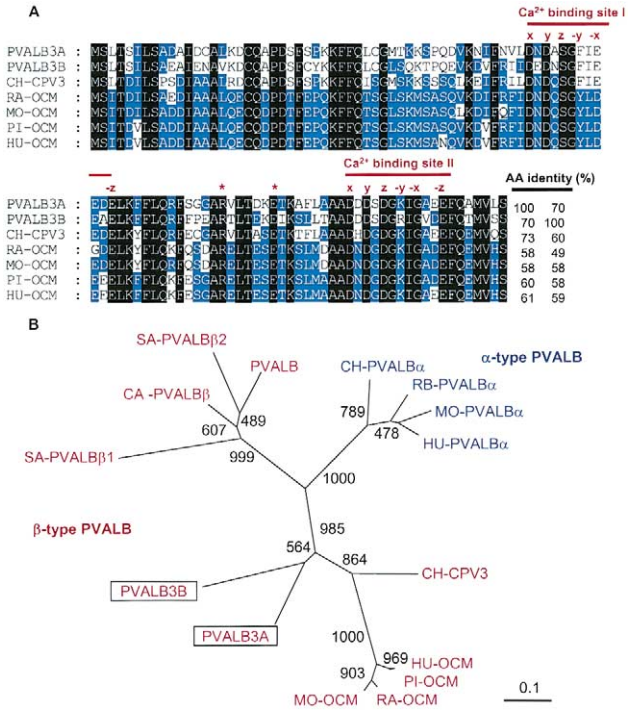

Fig. 1. (A) Alignment of amino acid sequences between zebrafish PVALB, chicken CPV3 and mammalian OCM. Residues conserved throughout the entire PVALB family are highlighted in black; residues conserved in at least 50% of the family members are highlighted in blue. Ca^{2+} binding domains are underlined. x, y, z, $-y$, $-x$ and $-z$ refer to the calcium-binding ligands arranged in approximately octahedral geometry around the metal ion (Kretsinger et al. 1991). Residues mediating salt-bridge formation are indicated by asterisks. The identities of the amino acid sequences are indicated in the lower right corner. (B) An un-rooted phylogenetic tree of PVALB based on amino acid sequences. The tree was constructed using the NJ method (Pearson et al., 1999) and the CLUSTAL W program (Thompson et al., 1994) with bootstrap values (based on 1000 iterations) shown at each node. Scale bar, genetic distance. Source: PVALB, zebrafish muscle-type PVALB (AAF78471); PVALB3A, zebrafish PVALB3A (AF425739); PVALB3B, zebrafish PVALB3B (AF425740); RA-OCM, rat OCM (PVRTO); MO-OCM, mouse OCM (I54105); HU-OCM, human OCM (XP_011576); CH-CPV3, chicken CPV3 (A53341); PI-OCM, pig-CBP15 (AAB61901); SA-PVALBβ2, salmon PVALBβ2 (Q91483); SA-PVALBβ1, salmon PVALBβ1 (Q91482); CA-PVALBβ, carp PVALBβ (PVCAB); HU-PVALBα, human PVALBα (PRVA_HUMAN); MO-PVALBα, mouse PVALBα (PRVA_MOUSE); RB-PVALBα, rabbit PVALBα (PRVA_RABIT); CH-PVALBα, chicken PVALBα (PRVM_CHICK).

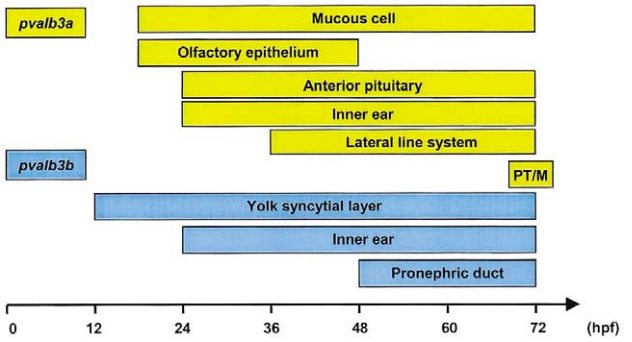

Fig. 2. Schematic representation of the spatio-temporal expression of *pvalb3a* (yellow) and *pvalb3b* (blue) detected by means of whole-mount in situ hybridization in zebrafish embryos. PT, pharyngeal teeth germ; M, macrophage.

1.2. Expression patterns of pvalb3a and pvalb3b

By reverse transcriptase-polymerase (chain reaction), neither *pvalb3a* nor *pvalb3b* expression was detected for oocytes or cleavage-stage embryos, thus excluding the possibility of maternal deposits of any *pvalb3a* and *pvalb3b* transcripts or a role for *pvalb3a* or *pvalb3b* in early embryogenesis (data not shown). We assayed the spatio-temporal expression of *pvalb3a* and *pvalb3b* through whole-mount in situ hybridization during embryonic development from 9 to 72 hours post-fertilization (hpf) (summarized in Fig. 2). The tentative expression pattern of each gene is described below, based on the time of appearance during embryogenesis.

1.2.1. Mucous cells

pvalb3a was initially detected in the mucous cells (Canfield et al., 2002) around 18 hpf (data not shown). From 24 hpf onward, the number of *pvalb3a*-expressing mucous cells increased rapidly (Fig. 3A), and they were widely and randomly distributed in the epidermis of the head (Fig. 3B), yolk sac, trunk and tail (Fig. 3C) at 36 hpf. However, the expression of *pvalb3a* in mucous cells was highly development-regulated. From 36 hpf onward, the expression of *pvalb3a* in mucous cells was sharply down-regulated in the trunk and was eventually only detectable in the mouth (Fig. 3P) and gill epithelium (Fig. 3D) at 72 hpf.

1.2.2. Olfactory epithelium

Olfactory placodes in zebrafish are formed by a subepidermal layer of cells at 14–16 hpf and differentiate into olfactory pits at 30–32 hpf (Hansen and Zeiske, 1993). The expression of *pvalb3a* was initially activated in all of the olfactory placodes at 18 hpf (Fig. 3E). By 36 hpf, the cucumber-shaped olfactory placodes filled the space between the eyes and the developing forebrain, and *pvalb3a* transcripts were robustly and uniformly expressed in the entire olfactory epithelium (Fig. 3F). By 48 hpf, *pvalb3a*-expressing cells in the olfactory epithelium remained positive in the apical surface, where the olfactory receptors and

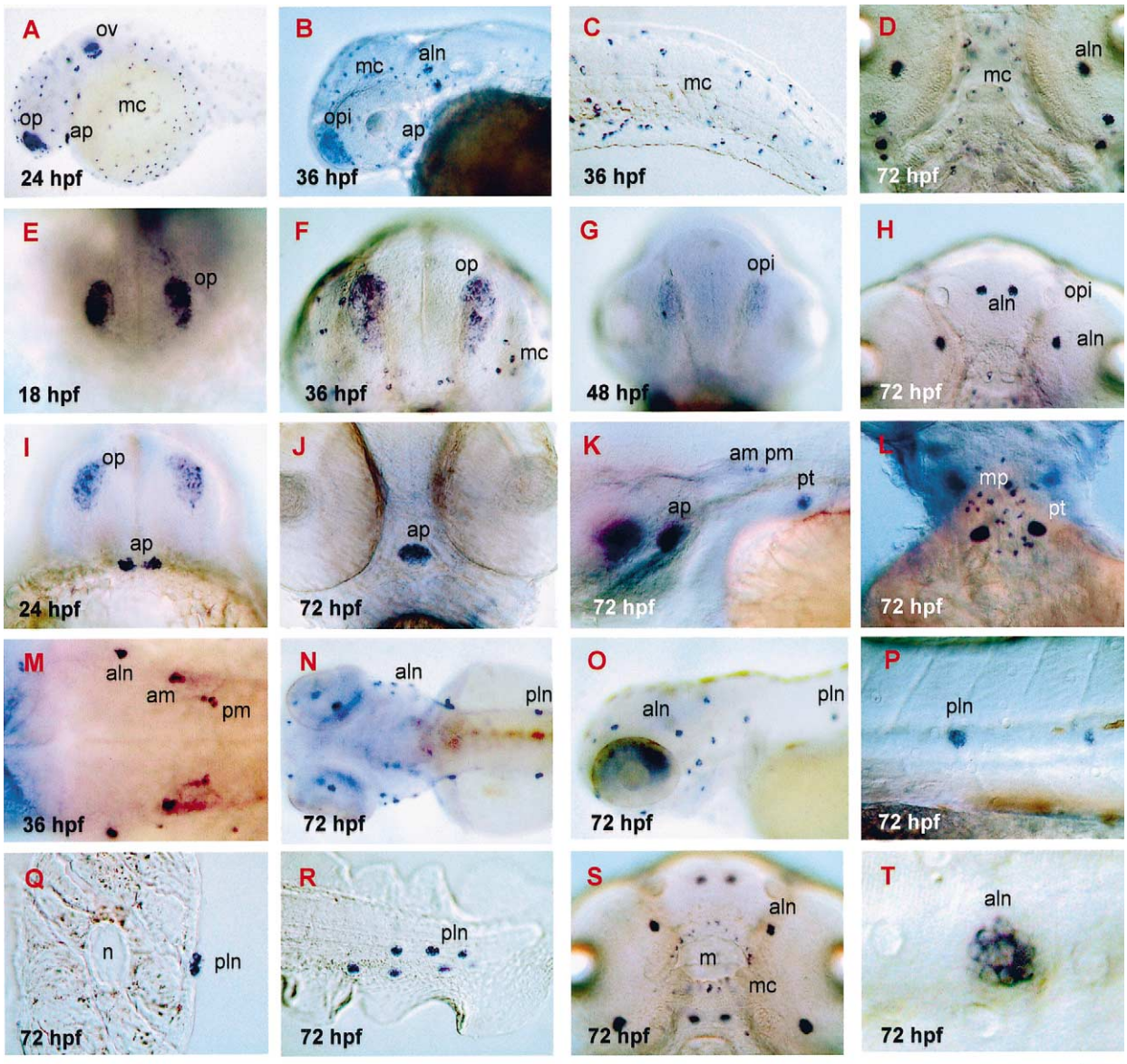

Fig. 3. *pvalb3a* expression during zebrafish embryogenesis. Lateral views (A–C,K,O,P,R,T), dorsal views (L–N), ventral views (D–J,S) and transverse section (Q) of whole-mount embryos following in situ hybridization for *pvalb3a*. Anterior is to the left in (A–C,K,M–P,R,T). Anterior is at the top in (D–J,L,S). (A–D) Expression of *pvalb3a* in mucous cells. (A) 24 hpf, mucous cells scattered in the epithelium of the entire embryo. Note that the olfactory placode, otic vesicle and anterior pituitary also express *pvalb3a*. (B) 36 hpf, mucous cells scattered in the epithelium of the head. Note that the olfactory placode, anterior pituitary and anterior lateral line neuromasts also express *pvalb3a*. (C) 36 hpf, mucous cells scattered in the epithelium of the tail and fin fold. (D) 72 hpf, mucous cells scattered in the gill epithelium. The larger *pavlb3a*-expressing cells surrounding the eyes are neuromasts of the infraorbital lines. (E–H) Expression of *pvalb3a* in the olfactory epithelium. All of the olfactory placodes (E, 24 hpf and F, 36 hpf) and olfactory pits (G, 48 hpf) are heavily and uniformly stained with *pvalb3a*. (H) 72 hpf, the entire olfactory epithelium of the nasal cavities is negative for *pvalb3a* staining. The larger *pavlb3a*-expressing cells near the nasal cavities and eyes are neuromasts of the infraorbital lines. (I–K) Expression of *pvalb3a* in the anterior pituitary. *pvalb3a* staining in the anterior pituitary initially appears as two clusters at 24 hpf (I), then fuses and shifts to the middle-posterior position between the two eyes at 72 hpf (J,K). (L) 72 hpf, expression of *pvalb3a* in pharyngeal teeth germs and macrophages. (M–T) Expression of *pvalb3a* in the lateral line system. (M) 36 hpf, *pvalb3a* is initially expressed in the matured neuromasts of the anterior lateral line system. At 72 hpf, all mature neuromasts in both the anterior (N,O,S,T) and posterior (P–R) lateral line systems robustly express *pvalb3a*. (P) 72 hpf, posterior lateral line neuromasts are deposited along the horizontal myoseptum. (Q) 72 hpf, transverse section at the level of the trunk, showing superficial distribution of *pvalb3a*-expressing neuromasts on the skin. The position of the notochord indicates the midline, with dorsal up. (R) 72 hpf, the last three neuromasts of the posterior lateral line system are also heavily stained with *pvalb3a*. (S) 72 hpf, *pvalb3a* transcripts are robustly expressed in the neuromasts of infraorbital lines. The smaller *pvalb3a*-expressing cells surrounding the mouth epithelium are mucous cells. (T) 72 hpf, high magnification of anterior neuromast showing that both sensory hair cells and supporting cells are *pvalb3a*-positive. aln, anterior lateral line neuromast; am, anterior maculae; ap, anterior pituitary; m, mouth; mc, mucous cell; mp, macrophage; n, notochord, op, olfactory placode; opi, olfactory pit; ov, otic vesicle; pln, posterior lateral line neuromast; pm, posterior maculae; pt, pharyngeal teeth germ. Scale bar = 140 μm in (A), 100 μm in (B,N,O), 50 μm in (C–M,P,R,S), 25 μm in (Q) and 12.5 μm in (T).

sensory neurons exist (Fig. 3G). From 48 hpf onward, *pvalb3a* transcripts were sharply down-regulated, and they were completely undetectable in the olfactory epithelium of the nasal cavity at 72 hpf (Fig. 3H).

1.2.3. Anterior pituitary, pharyngeal teeth germ and macrophages

PVALB3A and PVALB3B shared high sequence identities with chicken CPV3, which is exclusively expressed in the thymus (Hapak et al., 1994). The expression domain of both *pvalbs* in gland-related organ(s) is focused. Unlike chicken *CPV3*, zebrafish *pvalb3a* and *pvalb3b* transcripts were undetectable in the thymus. In the pituitary anlage, *pvalb3a*-expressing cells initially appeared as two separate cell masses around 24 hpf (Fig. 3I). From 36 hpf onward, *pvalb3a*-expressing cells in the pituitary anlage were fused, enlarged and shifted to the posterior region in relation to the head until they lay just behind the eye at 72 hpf (Fig. 3J, K). Compared to other pituitary markers, the expression of *pvalb3a* occurred about 4 h later than that of *eya1* (Sahly et al., 1999) and *lim3* (Glasgow et al., 1997). Thus, *pvalb3a* provides a marker for the migration and maturation processes of the anterior pituitary (adenohypophysis) in zebrafish. In addition, we also found two larger cell clusters (20 μm in diameter), located above the yolk sac and behind the otic vesicle, that also extensively expressed *pvalb3a* at 72 hpf (Fig. 3K, L). We concluded that these two *pavlb3a*-expressing cell clusters were pharyngeal teeth germs (Stock et al., personal communication). Interestingly, we also detected some macrophages that had accumulated in the pericardial cavity and expressed *pvalb3a* at 72 hpf (Fig. 3L).

1.2.4. Lateral line system

pvalb3a transcripts were first detectable in matured

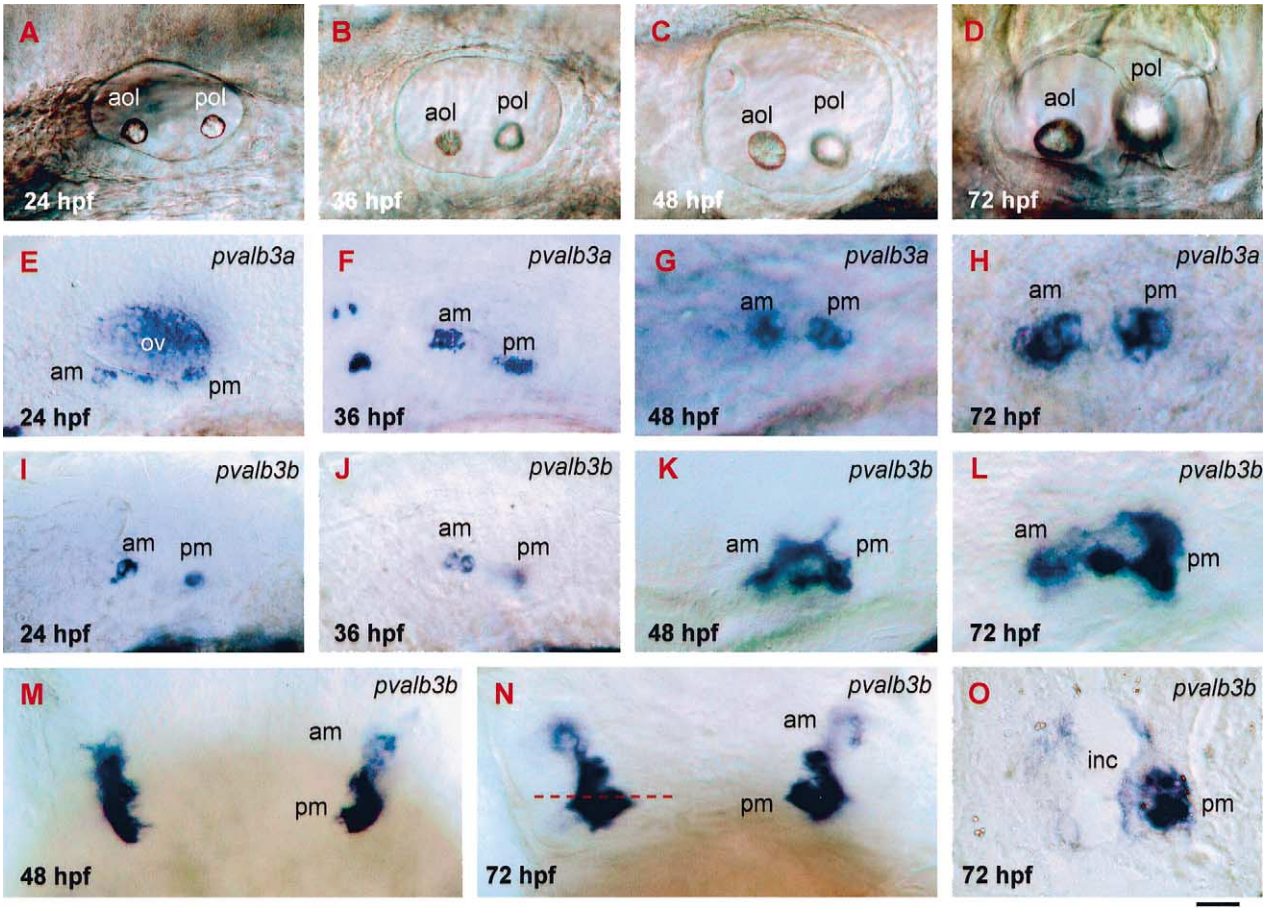

Fig. 4. *pvalb3a* and *pvalb3b* expression in the developing inner ears. Anterior is to the left in (A–L). Anterior is at the top in (M,N). Lateral views (A–L), dorsal views (M,N) and transverse section (O) of whole-mount embryos following in situ hybridization for *pvalb3a* (E–H) and *pvalb3b* (I–O). (A–D) Morphology of the inner ears in unfixed embryos at 24 hpf (A), 36 hpf (B), 48 hpf (C), and 72 hpf (D), showing the relative positions and sizes of two otoliths. (E–H) Expression of *pvalb3a* in the developing inner ears at 24 hpf (E), 36 hpf (F), 48 hpf (G), and 72 hpf (H). (I–O) Expression of *pvalb3b* in the developing inner ears at 24 hpf (I), 36 hpf (J), 48 hpf (K,M), and 72 hpf (L,N,O). Note the different distributions of *pvalb3a* and *pvalb3b* transcripts in the otic vesicle at 24 hpf and in the inner ear maculae after 48 hpf. Only *pvalb3a* is expressed in the otic vesicle at 24 hpf (E), and only the expression domain of *pvalb3b* extends into the surrounding non-sensory cells after 48 hpf (K–O) (dotted line indicates the plane of the section in O). (O) 72 hpf, transverse section at the level of the otic vesicle, showing *pvalb3b* expression in both sensory cells (maculae) and non-sensory cells surrounding the inner ear cavity (only the left side is shown). am, anterior maculae; aol, anterior otolith; inc, inner ear cavity; ov, otic vesicle; pm, posterior maculae; pol, posterior otolith. Scale bar = 25 μm in (A–N) and 10 μm in (O).

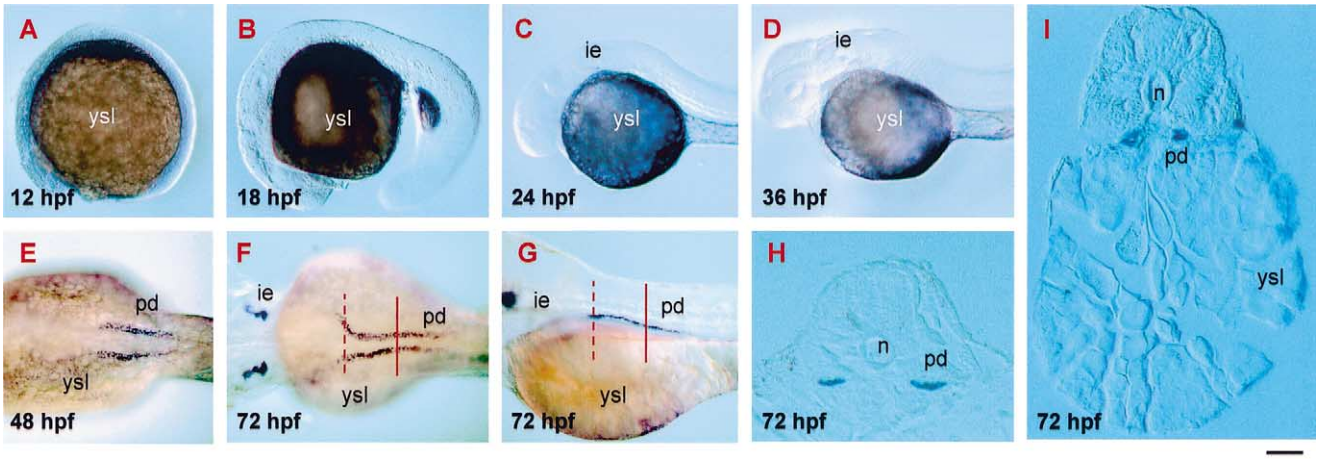

Fig. 5. *pvalb3b* expression during zebrafish embryogenesis. Anterior is to the left in (A–G). Lateral views (A–D,G), dorsal views (E,F) and transverse sections (H,I) of whole-mount embryos following in situ hybridization for *pvalb3b*. (A–D) Expression of *pvalb3b* in the yolk syncytial layer at 12 hpf (A), 18 hpf (B), 24 hpf (C), and 36 hpf. (D). (E) 48 hpf, expression of *pvalb3b* in the medial-posterior part of the pronephric ducts. (F,G) 72 hpf, expression of *pvalb3b* in the anterior part of the pronephric ducts (dotted and solid lines indicate the plane of the sections in H and I, respectively). (H) 72 hpf, transverse section at the level of the trunk, showing the bilateral distribution of *pvalb3b* transcripts in the anterior pronephric ducts. (I) 72 hpf, transverse section at the level of the trunk, showing *pvalb3b* transcripts in pronephric ducts and yolk syncytial layer. The position of the notochord indicates the midline, with dorsal up. ie, inner ear; n, notochord; pd, pronephric duct; ysl, yolk syncytial layer. Scale bar = 100 μm in (E–G), 70 μm in (A–D) and 25 μm in (H,I).

neuromasts of the otic line (Fig. 3M) and posterior lateral line (data not shown) around 36 hpf, but they could not be detected in the migrating lateral line primodium. By 72 hpf, *pvalb3a* were found to be robustly expressed in all the mature neuromasts of both the anterior (Fig. 3N, O, S, T) and posterior lateral line systems (Fig. 3P–R). Compared to hair cell-specific markers of *myosinVIIA* (Ernest et al., 2000) and *zath*1 (Itoh and Chitnis, 2001), *pvalb3a* transcripts were distributed in both sensory hair cells and surrounding supporting cells (Fig. 3T). Thus, *pvalb3a* demarcates mature hair cells and supporting cells in the lateral line system.

1.2.5. Inner ear

pvalb3a and *pvalb3b* shared overlapping but distinct expression domains in the developing inner ears. The activation time for both *pvalb3a* (Fig. 4E) and *pvalb3b* (Fig. 4I) in the inner ears was around 24 hpf, which coincided with the formation of hair cells in the maculae (Haddon and Lewis, 1996). By 24 hpf, *pvalb3a* transcripts were expressed in the entire epithelium of the otic vesicle and inner ear maculae, while *pvalb3b* transcripts were restrictedly expressed in the inner ear maculae. From 24 hpf onward, the expression of both *pvalb3a* (Fig. 4F–H) and *pvalb3b* (Fig. 4J–L) was up-regulated in the anterior and posterior maculae, which were the locations where further utricular and saccular maculae would form. From 48 hpf onward, however, *pvalb3b* (Fig. 4K–O) but not *pvalb3a* (Fig. 4G, H) transcripts extended their expression domains from hair cells into surrounding supporting cells and non-sensory regions around the inner ear cavity (Fig. 4O), resulting in two hook-like domains at 72 hpf (Fig. 4N).

1.2.6. Yolk syncytial layer and pronephric ducts

By 12 hpf, *pvalb3b* transcripts were appearing in the yolk syncytial layer, an extraembryonic tissue (Fig. 5A). From 12 hpf onward, *pvalb3b* transcripts were up-regulated in the yolk syncytial layer and showed uniform staining in both the yolk ball and yolk extension (Fig. 5B–D). From 48 hpf onward, *pvalb3b* was sharply down-regulated and showed faint staining in the yolk syncytial layer (Fig. 5E–G, I). Interestingly, OCM has been detected in extraembryonic tissues during early development in mammals (Brewer and MacManus, 1985). Thus, based on the evidence from expression analysis, we suggest that *pvalb3b* is more closely related to mammalian *OCM* than is *pvalb3a*. From 48 hpf onward, *pvalb3b* transcripts were also expressed in the developing kidney and showed faint staining signals in the medial–posterior pronephric ducts (Fig. 5E). By 72 hpf, however, *pvalb3b* was down-regulated in the medial–posterior pronephric ducts but up-regulated in the anterior pronephric ducts (Fig. 5F–H), while glomerulus, pronephric tubes and medial–posterior pronephric tubes lacked *pvalb3b* staining. The region-specific distribution of *pvalb3a* transcripts in the kidney was consistent with results detected in fish (Hearn et al., 1978; Gerday et al., 1979), *Xenopus* (Kerschbaum et al., 1994), rat (Bindels et al., 1991), and mice (Dai et al., 2001; Loffing et al., 2001) at the protein level. For example, in mice, PVALB is restrictedly distributed in the distal convoluted tubule, which is the primary site for transcellular magnesium reabsorption (Dai et al., 2001).

In summary, the expression of zebrafish *pvalb3a* and *pvalb3b* was distinct and highly development-regulated during early embryogenesis. Compared to their orthologues of *CPV3* in chicken and *OCM* in mammals, both *pvalb3a*

and *pvalb3b* not only share an evolutionarily conserved domain in sensory hair cells of the inner ear, but also have several additional expression domains usually detected in the α-type *pvalb*. *pvalb3a* transcripts are primarily associated with the development of neurogenic placodes-derived sensory organs (olfactory epithelium, inner ear and lateral line neuromasts) and somatic ectoderm-derived organs (mucous cells, anterior pituitary and pharyngeal teeth germ). *pvalb3b* transcripts, on the other hand, are more restrictedly distributed in the yolk syncytial layer, inner ears and pronephric ducts.

cDNA sequences of *pvalb3a* and *pvalb3b* have been deposited in the DDBJ/EMBL/GenBank databases with the accession number AF425739 and AF425740, respectively.

Acknowledgements

We gratefully thank Ajay Chitnis, Tom Finger, Anne Hansen, Kurt Kotrschal, David Stock, Bernard Thisse and Tanya Whitfield for helpful discussions. This work was supported by a grant from the National Science Council, Taiwan, ROC, under grant NCS90-2313-B-002-319.

References

Bindels, R.J., Hartog, A., Timmermans, J.A., van Os, C.H., 1991. Immunocytochemical localization of calbindin-D28k, calbindin-D9k and parvalbumin in rat kidney. Contrib. Nephrol. 91, 7–13.

Brewer, L.M., MacManus, J.P., 1985. Localization and synthesis of the tumor protein oncomodulin in extraembryonic tissues of the fetal rat. Dev. Biol. 112, 49–58.

Canfield, V.A., Loppin, B., Thisse, B., Thisse, C., Postlethwait, J.H., Mohideen, M.A., Rajarao, S.J., Levenson, R., 2002. Na,K-ATPase alpha and beta subunit genes exhibit unique expression patterns during zebrafish embryogenesis. Mech. Dev. 116, 51–59.

Dai, L.J., Ritchie, G., Kerstan, D., Kang, H.S., Cole, D.E., Quamme, G.A., 2001. Magnesium transport in the renal distal convoluted tubule. Physiol. Rev. 81, 51–84.

de Lecea, L., del Rio, J.A., Soriano, E., 1995. Developmental expression of parvalbumin mRNA in the cerebral cortex and hippocampus of the rat. Brain Res. Mol. Brain Res. 32, 1–13.

Endo, T., Takazawa, K., Onaya, T., 1985. Parvalbumin exists in rat endocrine glands. Endocrinology 117, 527–531.

Ernest, S., Rauch, G.J., Haffter, P., Geisler, R., Petit, C., Nicolson, T., 2000. Mariner is defective in myosin VIIA: a zebrafish model for human hereditary deafness. Hum. Mol. Genet. 9, 2189–2196.

Gerday, C., Joris, B., Gerardin-Otthiers, N., Collin, S., Hamoir, G., 1979. Parvalbumins from the lungfish (*Protopterus dolloi*). Biochimie 61, 589–599.

Glasgow, E., Karavanov, A.A., Dawid, I.B., 1997. Neuronal and neuroendocrine expression of lim3, a LIM class homeobox gene, is altered in mutant zebrafish with axial signaling defects. Dev. Biol. 192, 405–419.

Gosselin-Rey, C., Gerday, C., 1977. Parvalbumins from frog skeletal muscle (*Rana temporaria* L.). Isolation and characterization. Structural modifications associated with calcium binding. Biochim. Biophys. Acta 492, 53–63.

Haddon, C., Lewis, J., 1996. Early ear development in the embryo of the zebrafish, *Danio rerio*. J. Comp. Neurol. 365, 113–128.

Hansen, A., Zeiske, E., 1993. Development of the olfactory organ in the zebrafish, *Brachydanio rerio*. J. Comp. Neurol. 333, 289–300.

Hapak, R.C., Zhao, H., Boschi, J.M., Henzl, M.T., 1994. Novel avian thymic parvalbumin displays high degree of sequence homology to oncomodulin. J. Biol. Chem. 269, 5288–5296.

Hearn, P.R., Tomlinson, S., Mellersh, H., Preston, C.J., Kenyon, C.J., Russell, R.G., 1978. Low molecular weight calcium-binding protein from the kidney and gill of the freshwater eel (*Anguilla anguilla*). J. Endocrinol. 79, 36P–37P.

Henzl, M.T., Shibasaki, O., Comegys, T.H., Thalmann, I., Thalmann, R., 1997. Oncomodulin is abundant in the organ of Corti. Hear. Res. 106, 105–111.

Itoh, M., Chitnis, A.B., 2001. Expression of proneural and neurogenic genes in the zebrafish lateral line primordium correlates with selection of hair cell fate in neuromasts. Mech. Dev. 102, 263–266.

Kerschbaum, H.H., Singh, S.K., Hermann, A., 1994. Parvalbumin-immunoreactive material in the kidney of *Xenopus laevis*. Tissue Cell 26, 75–81.

Kretsinger, R.H., Tolbert, D., Nakayama, A., Pearson, W., 1991. The EF-hand, homologs and analogs. In: Heizmann, C.W. (Ed.). Novel Calcium Binding Proteins. Fundamentals and Clinical Implication, Springer, New York, NY, pp. 17–37.

Loffing, J., Loffing-Cueni, D., Valderrabano, V., Klausli, L., Hebert, S.C., Rossier, B.C., Hoenderop, J.G., Bindels, R.J., Kaissling, B., 2001. Distribution of transcellular calcium and sodium transport pathways along mouse distal nephron. Am. J. Physiol. Renal. Physiol. 281, F1021–F1027.

Pauls, T.L., Cox, J.A., Berchtold, M.W., 1996. The Ca^{2+}-binding proteins parvalbumin and oncomodulin and their genes: new structural and functional findings. Biochim. Biophys. Acta 1306, 39–54.

Pearson, W.R., Robins, G., Zhang, T., 1999. Generalized neighbor-joining: more reliable phylogenetic tree reconstruction. Mol. Biol. 16, 806–816.

Sahly, I., Andermann, P., Petit, C., 1999. The zebrafish eya1 gene and its expression pattern during embryogenesis. Dev. Genes Evol. 209, 399–410.

Sakaguchi, N., Henzl, M.T., Thalmann, I., Thalmann, R., Schulte, B.A., 1998. Oncomodulin is expressed exclusively by outer hair cells in the organ of Corti. J. Histochem. Cytochem. 46, 29–40.

Thompson, J.D., Higgins, D.G., Gibson, T.J., 1994. CLUSTAL W: improving the sensitivity of progressive multiple sequence alignment through sequence weighting, positions-specific gap penalties and weight matrix choice. Nucleic Acids Res. 22, 4673–4680.

Toury, R., Belqasmi, F., Hauchecorne, M., Leguellec, D., Heizmann, C.W., Balmain, N., 1995. Localization of the $Ca(^{2+})$-binding alpha-parvalbumin and its mRNA in epiphyseal plate cartilage and bone of growing rats. Bone 17, 121–130.